

ABSTRACT

8 This paper examines the physical controls of extratropical humidity and clouds by isolating the
9 effects of cloud physics factors in an idealized model. The Held-Suarez dynamical core is used with
10 the addition of passive water vapor and cloud tracers such that clouds do not feed back on circulation
11 or temperature, allowing cloud processes to be explored cleanly. Separate saturation adjustment
12 and full cloud scheme controls are used to consider the strength of advection-condensation theory.
13 Three sets of perturbation experiments are designed to test the model's sensitivity to the physics
14 of condensation, sedimentation, and precipitation formation. The condensation and sedimentation
15 perturbations isolate two key differences between the control cases. First, the sub-grid-scale relative
16 humidity distribution assumed within the cloud macrophysics scheme influences the location and
17 magnitude of the extratropical cloud maxima, limiting isentropic transport of tropical moisture
18 to the polar troposphere. Second, within the model's explicit treatment of cloud microphysics,
19 re-evaporation of hydrometeors moistens and increases clouds in the lower troposphere. While
20 these processes significantly control not only humidity and cloudiness, but also precipitation and
21 precipitation efficiency, microphysical processes of precipitation formation (specifically, the ratio
22 of accretion to autoconversion) have negligible effects on these indicators apart from the strength
23 of the large-scale condensation and formation cycle. Circulation sets the patterns of humidity,
24 clouds, and precipitation to first order, with factors explored herein providing secondary controls.
25 The results substantiate the utility of such idealized models for elucidating cloud processes in a
26 systematic manner and highlight key cloud processes to constrain.

27 **1. Introduction**

28 Cloud feedback is widely considered to be the largest contributor to the intermodel spread in
29 climate sensitivity among comprehensive General Circulation Models (GCMs) (e.g., Ceppi et al.
30 2017; Sherwood et al. 2020). Bony et al. (2015) argued that consensus among most comprehensive
31 GCMs does not, on its own, yield robust conclusions on cloud feedback. Rather, theories which
32 underpin physical arguments and improve understanding in a way that allows for expanded use
33 and interpretation of comprehensive GCMs are an additional requirement. Thus, simple models
34 whose workings can be clearly grasped play a key role in the midst of a complex scientific problem
35 (Pierrehumbert et al. 2007; Held 2005, 2014). If a GCM produces both observationally-constrained
36 cloud fields and multi-model consistent cloud feedbacks, but without the physical mechanisms
37 necessarily being represented appropriately, its prediction of the climatic response to a radiative
38 forcing may be significantly flawed. With the potential for unrealistic interactions between different
39 parameterized processes (Ceppi et al. 2017), decomposition of the effects of individual processes
40 could lead to improved parameterizations.

41 Here, we study under-constrained cloud macrophysical and microphysical processes by exploring
42 the underlying physical mechanisms. Since changing a stratiform cloud scheme can have significant
43 ramifications, even reversing a model's feedback with warming (Geoffroy et al. 2017), we use an
44 idealized setup to break down a cloud scheme and understand the effects of individual cloud
45 processes on atmospheric humidity and cloudiness. The processes studied herein are motivated by
46 three factors: understanding the differences between the advection-condensation theory of humidity
47 and a cloud scheme, the controls of precipitation efficiency, and the direct effect of stratiform-cloud
48 related GCM parameters on free tropospheric humidity and clouds.

49 *a. Advection-Condensation Theory*

50 Free tropospheric humidity is important to the distribution of clouds and precipitation. The
51 so-called advection-condensation theory suggests that water vapor (WV) in the atmosphere is most
52 simply reflective of the lowest temperature (lowest saturation specific humidity) experienced by
53 the parcel since leaving the nearly saturated surface layer. This theory alone can describe WV
54 distribution to first order (Sherwood et al. 2010). Advection-condensation theory helps explain
55 two key features of free tropospheric humidity: dry subtropical zones and moist polar regions
56 connected by dry isentropes.

57 Pierrehumbert (1998) laid out three factors which contribute to the dry subtropics. First, sub-
58 sidence brings down dry air, and would keep the region at the mixing ratio of the tropopause if
59 not for other mechanisms. Second, lateral mixing brings in moist air from the tropical convective
60 region. Third, processing of air through cold extratropics dries the region. Thus, the dry subtropics
61 and moist poles are connected through nearly isentropic large-scale advection, and cycling through
62 cold polar upper tropospheric air is a key means of dehydrating air in the extratropics (Kelly et al.
63 1991). Finally, Pierrehumbert (1998) also noted the role of re-evaporation of hydrometeors as
64 a subtropical moisture source as emphasized by Sun and Lindzen (1993), but suggested this is
65 limited by weak rainfall. Also suggesting the importance of in situ moistening processes in the
66 midlatitudes, Yang and Pierrehumbert (1994) showed that in the advection-condensation model,
67 the tropical moisture source is too inefficient (that is, too weak of mixing between tropics and
68 extratropics). These factors have been expounded in further work.

69 Using a simple saturation adjustment scheme as a representation of advection-condensation the-
70 ory, Galewsky et al. (2005) found that the primary dynamical control of the dry subtropics was
71 isentropic dehydration by mid-latitude eddies (with diabatic descent through Hadley circulation

72 playing a secondary role). WV is transported from the lower deep tropics to the upper polar extrat-
73 ropics by baroclinic eddies along isentropes, with the moist air rising and cooling adiabatically. The
74 storm tracks interrupt the transport such that significant moisture is released through precipitation
75 before reaching the poles. Thus, the return flow supplies dehydrated air to the subtropics, and is
76 confined to isentropic layers (Held and Schneider 1999). The poleward eddy WV transport follows
77 dry isentropes but different values of equivalent potential temperature, with this moist recirculation
78 peaking on the equatorward side of the storm tracks (Laliberté et al. 2012). In this study, we
79 consider how a cloud scheme distributes moisture differently than simple saturation adjustment (as
80 in Galewsky et al. 2005), and we highlight the processes—cloud macrophysics and microphysics
81 alike—that affect extratropical humidity strongly. The physical mechanisms of these controls are
82 delineated to highlight those processes that need to be represented accurately in cloud schemes.

83 *b. Precipitation Efficiency Controls*

84 Differences between saturation adjustment and a cloud scheme are closely related to the con-
85 trols of precipitation efficiency. The residence time of water in the atmosphere is, in a full cloud
86 scheme, affected by three efficiencies: the efficiency with which WV may become cloud conden-
87 sate (condensation), become part of a falling hydrometeor (formation), and reach the surface as
88 precipitation (sedimentation) (Langhans et al. 2015). Advection-condensation theory reduces this
89 complexity to one efficiency since WV in excess of saturation immediately becomes surface pre-
90 cipitation. Thus, condensation and sedimentation efficiencies highlight two of the key differences
91 between a saturation adjustment scheme (based on advection-condensation theory) and a full cloud
92 scheme (closer to reality): condensation efficiency is affected by assumptions of small (sub-grid)
93 scale RH distribution, and sedimentation efficiency by re-evaporation of precipitation. The third
94 efficiency—formation efficiency—can be affected by internal cloud scheme parameters such as the

95 assumed cloud condensation nuclei (which affects warm rain processes) or the fall speed of ice.
96 But each of the three efficiencies have the potential to significantly affect WV and cloud condensate
97 (CC) fields, the distribution of precipitation, and the overall residence time of atmospheric water.
98 For example, precipitation efficiency (the multiplicative product of formation and sedimentation
99 efficiencies) is frequently highlighted as being potentially affected by creating more liquid at the
100 expense of ice in mixed-phase clouds (Klein et al. 2009; McCoy et al. 2015; Ceppi et al. 2016;
101 McCoy et al. 2018). Here we explore the direct effect of changing these efficiencies on steady-state
102 fields which are relevant to radiative feedbacks.

103 *c. GCM Stratiform Tuning Parameters*

104 Thus the first two motivations are connected to the third of the direct effect of stratiform-cloud
105 related GCM tuning parameters on free tropospheric humidity and clouds. Critical RH (the
106 minimum GCM grid-box-mean RH needed for cloud condensate formation) is a useful tuning
107 parameter for radiative balance (through shortwave cloud radiative effects), but may be tuned
108 artificially high in order to compensate for too-bright clouds (McCoy et al. 2016). Critical RH is
109 important because it controls large-scale condensation, a sink of WV and source of CC. WV can
110 be altered without directly affecting CC by tuning the re-evaporation of precipitation. Another key
111 parameter is N , the assumed cloud drop number concentration: aerosols affect microphysics and
112 thus precipitation and radiation through aerosol-cloud interactions. The observed precipitation rate
113 can be expressed as a power-law function of LWP and N , with a strong correlation between LWP
114 and the ratio of accretion to autoconversion processes (hereafter $accr/_{auto}$; Jiang et al. 2010). At
115 low LWP, $accr/_{auto}$ is small because of few generated rain drops. Some GCMs directly model
116 aerosol indirect effects, but even in simpler cloud microphysics schemes which lack an explicit
117 representation of aerosol indirect effects, the autoconversion process is a direct function of N

118 and thus a major control of $accr/auto$, which is a key parameter for examining the balance of
119 microphysical conversion processes from cloud water to rainwater (e.g., Gettelman et al. 2013).

120 In a GCM study implementing five different autoconversion schemes, Michibata and Takemura
121 (2015) found significant variance in $accr/auto$. But, these schemes showed a commonality of
122 the relative role of the accretion process being one or more orders of magnitude underestimated
123 compared to observations (as estimated by Gettelman et al. 2013). This incorrect ratio comes
124 from both too high simulated autoconversion rates (Gettelman et al. 2013, 2014) and in some
125 schemes, too low of an accretion enhancement factor for correct precipitation intensity (Wu et al.
126 2018). The high simulated autoconversion rates come from diagnostic precipitation which forms
127 warm rain too easily (Jing et al. 2017). Cloud condensation nuclei and $accr/auto$ affect not only
128 precipitation rates but also radiative forcing. Gettelman et al. (2013) noted a strong increase in
129 LWP with simulated $accr/auto$ (as in observations), and cloud optical depth and thus shortwave
130 radiative effect is significantly controlled by LWP (e.g., Stephens 1978). As past studies have likely
131 underestimated the true sensitivity of clouds and radiation to aerosols, the negative forcing of the
132 Twomey effect (altered cloud albedo from increased anthropogenic aerosols) may be underestimated
133 (Quaas et al. 2020). Yet, Gettelman et al. (2013) suggested that the autoconversion rate bias can be
134 corrected by altering the relative balance of the autoconversion and accretion rates, which lowers
135 the radiative effect of aerosol cloud interactions. Thus, understanding the interplay and impacts of
136 altered N and $accr/auto$ is critical.

137 *d. Purpose and Organization*

138 The overarching purpose of this paper is to employ an idealized model setup to shed light on what
139 controls free tropospheric humidity and cloudiness. Using perturbation experiments which isolate
140 key processes, we aim at elucidating the complex connections among WV, clouds, precipitation,

141 and circulation. In analyzing the control and perturbation experiments in this study, the budgetary
142 terms of the cloud scheme which represent the conversions among WV, CC, and precipitating
143 water (P) are particularly emphasized. This method is motivated by a need for a robust physical
144 understanding to ground model representations of cloud processes in order to lend confidence to
145 model-inferred relationships (Shepherd 2014; Stevens and Bony 2013).

146 A process-based analysis is related to the secondary purpose of this work: to clearly demonstrate
147 the value of this modeling tool (a dry GCM with passive water and cloud tracers) for developing a
148 systematic understanding of physical controls on humidity and clouds and diagnosing their repre-
149 sentations in models. This approach is in the same spirit as “mechanism-affirmation experiments”
150 described in Jeevanjee et al. (2017) as being the provision of a model hierarchy framework. In
151 terms of the model hierarchy, the setup used in this paper (Ming and Held 2018) is derived from the
152 Held-Suarez (HS) dry GCM, but in a different direction than the Frierson moist aquaplanet GCM
153 (Frierson et al. 2006) which extended the HS dry GCM by adding a gray radiation scheme and moist
154 physics such that latent heating affects the model’s dynamics. Our model is in many aspects more
155 idealized than the Frierson model with dry dynamics and no radiation scheme, but more complex
156 in its addition of a full cloud microphysics scheme. It can be thought of as one rung higher on the
157 model hierarchy ladder than the HS dry GCM, but one rung lower than the Frierson model. This
158 setup is therefore uniquely suitable for answering specific questions about extratropical humidity
159 and cloudiness—namely the direct effects of cloud macrophysics and microphysics—as well as the
160 physical mechanisms behind these effects.

161 This paper is organized as follows. Section 2 lays out the methodology of this study, describing
162 the idealized model, experiments, and analysis framework. Section 3 describes the results from the
163 control saturation adjustment and cloud physics experiments and the condensation, sedimentation,
164 and formation perturbations. Section 4 discusses the implications of these results for the value of

165 the advection-condensation paradigm, key stratiform cloud physics processes to constrain, and the
166 utility of this idealized model.

167 **2. Methodology**

168 *a. Control Models*

169 The idealized model used here is based on the HS dry GCM (Held and Suarez 1994) with the
170 addition of four passive water and cloud tracers—specific humidity, cloud liquid, cloud ice, and
171 cloud fraction (CF)—as described in Ming and Held (2018). The dry GCM uses a hydrostatic
172 spectral dynamical core for an ideal gas atmosphere with no topography. For this work, a resolution
173 of T42 (referring to the maximum number of zonal waves present in the triangular truncation) is
174 used, resulting in a horizontal grid of 128 by 64 cells (about 2.8° spacing) with 20 vertical layers
175 equally spaced in the sigma coordinate. The forcing consists of Newtonian relaxation of temperature
176 toward a prescribed zonally symmetric equilibrium temperature and planetary boundary layer drag
177 represented by Rayleigh damping. This idealized setup enables the isolation of the roles of various
178 cloud processes. It assumes that latent heating or cooling from conversions among WV, CC, and
179 precipitation do not feed back on the dynamics. Also, with no explicit radiation scheme in the
180 model, clouds do not affect circulation through cloud radiative effects. Thus, WV and clouds are
181 passive in that they do not affect circulation or temperature patterns.

182 Two control simulations are created with results explored in section 3a. The first, referred to as
183 the *Base* case, uses only the specific humidity tracer in a saturation adjustment scheme modeled
184 after Galewsky et al. (2005) as a direct representation of advection-condensation theory. Any water
185 in excess of saturation is assumed to fall out immediately as precipitation. Thus, no clouds are
186 present. The second control simulation is referred to as the *Cloud* case. It carries specific humidity,

187 cloud liquid, cloud ice, and CF tracers through the same large-scale cloud scheme as implemented
188 in the GFDL HiRAM model (Zhao et al. 2009). The cloud scheme assumes a beta distribution
189 for sub-grid-scale total water (which includes both WV and CC). CF is diagnosed from this total
190 water-based RH, which varies only slightly from traditional RH (which is based on WV only and
191 is the RH reported in the results). The default beta distribution is such that a grid-mean total
192 water-based RH value exceeding 83.3% (the critical RH: RH_c) allows for sub-grid values greater
193 than 100% and thus a non-zero CF for the grid box.

194 The pathways for conversion between WV, cloud liquid, cloud ice, and hydrometeors follow a
195 Rotstayn-Klein single-moment microphysics scheme (after Rotstayn 1997; Rotstayn et al. 2000).
196 Additionally, as the principal source of WV, surface evaporation is represented by adjusting the
197 specific humidity of grid boxes below ~ 850 hPa towards saturation with an e-folding timescale of
198 30 minutes. Microphysical sources of WV are large-scale (LS) evaporation of cloud liquid, LS
199 sublimation of cloud ice, rain evaporation, and snow sublimation. The only sinks of WV, namely
200 LS condensation and LS deposition, are also the only sources of CC. CC is lost to WV through LS
201 evaporation and LS sublimation, to rain through autoconversion, accretion, and melting of cloud
202 ice, and to snow through gravitational settling. Additionally, cloud liquid is converted to cloud ice
203 through riming, the Bergeron-Findeisen process, and homogeneous freezing, and both cloud ice
204 and snow can be converted to rain through melting. See Fig. 1 in ? and the descriptive text for
205 more details of these conversions.

206 *b. Perturbation Experiments*

207 On the surface, there are three chief distinctions between saturation adjustment (Base control)
208 and a full cloud scheme (Cloud control). First, clouds can form (and thus precipitation is possible)
209 before the grid box is fully saturated through RH_c and an assumed sub-grid-scale RH distribution.

210 Second, the cloud scheme allows precipitation to evaporate before reaching the surface through
211 rain evaporation and snow sublimation (hereafter RESS). Third, cloud condensate may be advected
212 before precipitating out or evaporating. The effects of the first two distinctions can be easily explored
213 by being simply "turned-off" in the cloud scheme. The third is inferred as a residual effect.

214 Each of the three distinctions correspond to the three efficiencies which effect the residence time
215 of water in the atmosphere and form a key part of the analysis. We make use of the explicit/large-
216 scale precipitation efficiency (PE) as defined in Zhao (2014) to represent the total PE, since only
217 stratiform (not convective) precipitation is represented in this model. PE is the ratio of surface
218 precipitation to CC sources (condensation and deposition), and thus represents the fraction of
219 condensed particles which subsequently rain out. Following Langhans et al. (2015), PE can be
220 thought of as the product of a formation efficiency (FE) and a sedimentation efficiency (SE). A
221 molecule of WV in the atmosphere may become CC condensate (condensation), become part
222 of a falling hydrometer (formation), and reach the surface as precipitation (sedimentation). FE
223 represents the probability of formation given condensation, and SE represents the probability
224 of sedimentation given formation. Finally, the condensation efficiency (CE) is the probability
225 of condensation given entrainment into a cloud but is used herein to represent the fraction of
226 atmospheric WV that subsequently condenses. Thus, CE is the ratio of CC sources to WV sources,
227 FE is the ratio of precipitation formation to CC sources, and SE is the ratio of surface precipitation
228 to precipitation formation. Additionally, the residence (or recycling) time for WV in the atmosphere
229 is defined after Trenberth (1998) as the e -folding time constant for the depletion of precipitable
230 water by precipitation, that is, the global ratio of column-integrated WV to the precipitation rate.
231 These indicators of features of the water cycle are used to quantify changes in the WV, CC, and
232 precipitation budgetary terms to supplement the analysis of steady-state fields. But also, as these
233 efficiencies correspond to distinctions between saturation adjustment and a cloud scheme, we

234 intentionally alter the efficiencies to understand the effects on steady-state fields. CE is affected by
235 RH_c , SE is 100% without RESS, and FE cannot be defined without CC.

236 Thus, three principal perturbation experiments are designed, testing sensitivity to condensation,
237 sedimentation, and formation cloud processes. The condensation perturbation focuses on the con-
238 version between WV and CC through cloud macrophysics, specifically sub-grid-scale cloudiness.
239 The first key distinction between saturation adjustment and a cloud scheme can be eliminated
240 by removing sub-grid-scale cloudiness and requiring 100% grid-mean RH for cloud formation.
241 Accordingly, an intermediate setup between the Base and Cloud controls is created by reducing the
242 width parameter of the beta distribution defining sub-grid-scale RH from 0.2 to 0.01, effectively
243 requiring 100% grid-box-mean RH for cloud formation. This perturbation run is referred to as
244 *RHc100* (since effectively $RH_c = 100\%$) with results in Section 3b.

245 The sedimentation perturbation focuses on the role of re-evaporation of hydrometers. While
246 saturation adjustment oversimplifies the variety of conversions in this Rotstayn-Klein microphysics
247 scheme, it is analogous to the LS phase changes and precipitation processes. The chief remaining
248 processes are the recycling of hydrometeors back to WV through RESS. Thus, another intermediate
249 setup between the controls is created to illuminate the significance of RESS. For this experiment—
250 *noRESS* which is presented in Section 3c—the rates of RESS are arbitrarily set to zero. Additionally,
251 to examine the combined effect of the key microphysical and macrophysical differences between
252 the Base and Cloud cases, a final intermediate case is considered. The *RHc100_noRESS* case
253 includes the $RH_c = 100\%$ and omission of RESS effects to examine residual differences between
254 the control cases, which is assumed to correspond to the third key difference between saturation
255 adjustment and full cloud physics—advection of CC—as explored in Section 4.

256 The formation perturbation is not focused directly on a difference between the Base and Cloud
257 cases. In the Base case saturation adjustment, precipitation is formed directly from WV in a manner

258 more similar to condensation than formation. Rather, formation is explored so that sensitivity to
259 all key conversions of the cloud scheme are considered. Formation consists of three major process:
260 autoconversion, accretion, and ice settling. Ice settling is a net term—the difference between ice
261 falling into and out of grid boxes. Accordingly, autoconversion and accretion were isolated as the
262 best processes to perturb in order to explore formation sensitivities. From a general perspective,
263 if autoconversion or accretion is arbitrarily reduced in this model, the other process strengthens to
264 keep formation close to constant, but somewhat reduced. Conversely, if one process is amplified,
265 the other weakens. An analogous effect results from altering the prescribed cloud drop number
266 concentration, N , the default value being 50 m^{-3} , since both autoconversion and accretion are
267 a function of N . For autoconversion to occur, the radius of the cloud droplets—a function of
268 N —must be greater than the critical particle radius threshold at which autoconversion occurs. For
269 accretion, the collection efficiency of a cloud droplet by a liquid droplet is a function of particle
270 size which is a function of N . If N is decreased, autoconversion increases and accretion decreases
271 with a net amplification of formation. An increase of N produces an a opposite effect. Thus,
272 the strength of formation and the balance between autoconversion and accretion have broader
273 significance because of their connection to drop number concentration parameterizations.

274 Here, alterations to autoconversion are used to adjust *accr/auto* (and indirectly explore a key
275 affect of altered N). The principal formation perturbation explored in Section 3d, *halvAUTO*,
276 consists of halving the computed value for autoconversion for each grid box at each time-step. For
277 robustness, a corresponding doubling of of autoconversion, *doubAUTO* is also examined. Note
278 that the halving or doubling of autoconversion is performed in the microphysical code before the
279 enforcement of a limiter which ensures that autoconversion is limited to the amount that reduces
280 local liquid cloud condensate to the critical value at which autoconversion begins (after Rotstayn
281 1997).

282 For all control and perturbation experiments, the atmospheric state of the model (winds, temper-
283 ature, etc.) is identical at every time-step. The various experiments performed are summarized in
284 Table 1. All model runs in this study include a 300-day spin-up of the dry GCM before the next
285 1000 days are averaged. For figures and analysis, data is averaged between the two hemispheres
286 because of the hemispheric symmetry of the simulated climate. 15° to 90° is considered the sub-
287 and extra-tropics (STET) and is the focus of the analysis due to the lack of a convection scheme
288 making the tropics nearly saturated (see Ming and Held 2018).

289 **3. Results**

290 *a. Controls: Base and Cloud*

291 A budgetary comparison of the control cases is shown in Fig. 1a, which depicts the principal
292 WV tendency terms for the Base and Cloud cases from a column-integrated, zonally-averaged
293 perspective. For the Base case, the WV balance is simply between precipitation from saturation
294 adjustment and surface evaporation. Outside of the tropics (which are not shown), the immediate
295 precipitation dominates in the mid-latitude storm tracks while evaporation occurs mostly in the
296 subtropics, implying significant horizontal advection of water from the subtropics (including
297 that facilitated by mid-latitude baroclinic eddies). For the Cloud case, the dominant balance
298 between net LS condensation (condensation and deposition minus evaporation and sublimation
299 with condensation dominating) as the main WV sink and surface evaporation as the main WV
300 source is similar to the Base case, though RESS does make a non-negligible contribution. Cloud
301 case LS condensation is everywhere stronger than Base case saturation adjustment, while the surface
302 evaporation is nearly indistinguishable except in the high latitudes where Base surface evaporation
303 is negligible. Thus, RESS provides an additional source of WV, strengthening the WV cycle as

304 opposed to replacing surface evaporation as a source. Fig. 1b shows the CC budget applicable
305 only to the Cloud case. Net LS condensation as the source of CC is balanced nearly perfectly
306 latitudinally, implying minimal advection of CC. In the subtropics, autoconversion dominates
307 accretion and ice settling as sinks of CC, but ice settling (snow) dominates poleward of 40° with
308 rain processes becoming negligible poleward of 60°.

309 While precipitation is simply saturation adjustment in the Base case but formation processes
310 minus RESS in the Cloud case, both precipitation and precipitation minus evaporation (P-E) have
311 similar latitudinal distributions in the two cases (Fig. 1c). The principal latitudinal difference is
312 a slight increase in precipitation (and thus P-E) in the extratropics in the Cloud case, where ice
313 settling (a process vastly different than saturation adjustment) dominates as the principal source of
314 precipitation, and surface evaporation decreases in the Base case as discussed previously. Thus,
315 the strength of the hydrological cycle in terms of surface precipitation is largely indistinguishable
316 with a STET average of 1.84 mm/day in the Base case and 1.91 mm/day in the Cloud case (see
317 Table 2 which also shows a similarity in surface evaporation). This correspondence between these
318 idealized saturation adjustment and full cloud microphysics models without any control by radiative
319 balance suggests a significant control of the hydrological cycle by large-scale circulation perhaps
320 mediated through RH (as discussed below).

321 In contrast, the strength of the WV cycle differs greatly between the two control cases. This can
322 be seen in Fig. 2a and b which depict the globally-averaged, column-integrated values and fractions
323 of the sources and sinks in the Base and Cloud cases. The total STET WV sources and sinks in the
324 Cloud case are 3.63×10^{-5} and 2.82×10^{-5} $\text{kg m}^{-2} \text{ s}^{-1}$, respectively, with the regional imbalance
325 implying advection of WV into the tropics (since evaporation is strongest in the subtropics). For
326 comparison, the Base case analogs of surface evaporation (the only WV source) and condensation
327 (the only WV sink) are 2.70×10^{-5} and 2.11×10^{-5} $\text{kg m}^{-2} \text{ s}^{-1}$, respectively. Thus, the strength of

328 the cycling of WV is significantly enhanced in the Cloud model by $\sim 30\%$. Adding more sources
329 and sinks of WV, in particular introducing sources above the boundary layer through RESS, allows
330 for a strengthening of the WV cycle and a slight shortening of the residence time (from 13.1 to
331 12.7 days). In the Cloud case, CC is also cycled where all the WV sinks are CC sources, and
332 precipitation processes are the main CC sinks (see Fig. 2b) with CC sources and sinks balanced in
333 the STET region.

334 This overall picture of water cycling between WV, CC, precipitation, and an assumed surface
335 reservoir can be seen in Fig. 3 and described in terms of efficiencies. For the STET WV produced
336 through surface evaporation, RESS, and evaporation (LS evaporation and sublimation), 83.9%
337 is condensed (through LS condensation and deposition). Of the water condensed, most forms
338 precipitation, while some is evaporated resulting in a FE of 98.2% . (Some also persists as
339 condensate but this effect is lost with time-averaging). Of the precipitation formed, $\sim 20\%$ is
340 returned to WV through RESS before reaching the surface resulting in an SE of 79.7% and a PE of
341 78.3% . These efficiencies, along with precipitation and residence times, are summarized in Table
342 2. The positive WV reservoir and negative surface reservoir value are again indicative of moisture
343 export (negative P-E) from the STET region.

344 A comparison of RH in the Base and Cloud cases is shown in Fig. 4a. The Base RH has qual-
345 itatively realistic free tropospheric features: the subtropics and upper troposphere are relatively
346 dry, while the extratropics are moist (Fig. 4a). As noted in Ming and Held (2018), the high RH
347 values in the deep tropics (not shown) and boundary layer (below 850 hPa) are due to the lack
348 of a moist convection scheme and the way in which surface evaporation is modeled, respectively.
349 Fig. 4a suggests that the addition of a cloud scheme has two main effects on the RH distribution,
350 while keeping the main features present. The subtropical dry zones and nearby mid-latitudes are
351 significantly moistened with a peak increase of up to around 5% RH, while much of the polar

352 upper troposphere becomes drier by a similar magnitude. The mechanisms for these changes are
353 investigated in the condensation and sedimentation perturbations. Fig. 4b shows the model isen-
354 tropes, significant because of the established isentropic transport of moisture from the subtropics as
355 discussed in the introduction. Here, it is clear that the polar upper troposphere (drier in the Cloud
356 case) is connected to the the subtropical boundary layer via isentropes. Yet, the overall similarity
357 between the control cases in the free troposphere implies that RH is controlled to first order by
358 general circulation, as opposed to cloud processes. Thus, in keeping with advection-condensation
359 theory, one does not need detailed cloud information for understanding large-scale RH patterns.

360 The cloud fields generated in the Cloud case are shown in Fig. 4c-d. Free tropospheric CF values
361 peak at near 30% in the extratropical storm track region, co-incident with the 75% average RH
362 contour. Liquid cloud condensate (LCC) is concentrated in the boundary layer with a secondary
363 peak near the storm tracks. Ice cloud condensate is concentrated in a broad region near the storm
364 tracks restricted to freezing temperatures (see Fig. 4b). LCC, with its higher magnitude, dominates
365 the spatial pattern of total CC), which is the sum of ice and liquid water mixing ratios. Since the
366 focus of this study is on total clouds, not on the distribution of ice versus liquid, the remainder of
367 this work will consider only total CC, which is concentrated in the tropics with a secondary peak
368 in the storm tracks.

369 *b. Condensation Perturbations: RHc100*

370 As discussed in the introduction, since isentropic transport is the key source of WV for the polar
371 regions, cloud formation (and precipitation) in the extratropical storm tracks provides a limiting
372 effect on the amount of WV reaching the polar regions. In the Cloud case, cloud formation
373 (required for precipitation) takes place when grid-mean RH (as defined by total water) exceeds
374 83.3%. Therefore one might expect a correlation between the model's extratropical cloud maxima

375 (storm tracks) in the model and 83.3% RH contours. But cloud formation is based on instantaneous
376 RH, not the long-term averages shown in Fig. 4c where the storm tracks are roughly co-located
377 with the 75% RH contours. Higher RH values may occur equatorward of a given RH contour.
378 Allowing for time variability in RH renews the possibility of a connection between the location of
379 the storm tracks and RH distribution because of RH_c . This possible connection is explored with
380 the RHc100 run, where the cloud scheme is adjusted to require essentially 100% grid-mean RH
381 for cloud formation.

382 In the RHc100 case, the entire WV/CC cycle slows down significantly compared to the Cloud
383 case (see Fig. 2b and c). Since clouds are now unlikely to form and remove moisture from the
384 atmosphere below 850 hPa (where the air is generally nearly, but not quite, saturated), surface
385 evaporation decreases (Fig. 5a). RESS play less of a role as WV sources, approximately half of
386 both the magnitude and percentage as in the Cloud case, and become nearly non-existent in the
387 extratropics. LS condensation decreases as a WV sink and CC source; the slowdown increases the
388 WV residence time by 2.6 days or 13% (Table 2).

389 CE decreases only slightly (3%) despite the intense perturbation in condensation. CE is not a
390 measure of how fast WV condenses, but simply whether it eventually does (in the given region
391 which here is the STET region). Similarly, FE decreases by 3% with a greater weakening of
392 formation processes than condensation (see Fig. 5b). FE represents the likelihood that a water
393 molecule, once it condenses, forms precipitation. Here, FE decreases since LS evaporation and
394 sublimation have increased both in value and as a percentage of LS condensation/deposition. In the
395 RHc100 setup, once a cloud is formed, if it persists to another time-step where RH has decreased
396 (as from precipitation), the remaining cloud condensate must entirely re-evaporate/sublimate. In
397 contrast, in the Cloud case, only enough cloud condensate to match the RH-based PDF must
398 evaporate, as long as grid-box-mean RH is above 83.3%.

399 The most significant change in efficiencies is SE which increases from 79.7% to 89.4% resulting
400 in an amplification in PE from 78.3% to 85.1%. SE increases because of the drastic decrease in
401 RESS. Like RESS, precipitation formation (Fig. 5c) declines everywhere with a resulting 10%
402 reduction in STET surface precipitation (Table 2). The precipitation decrease is proportionally
403 most significant in the high latitudes beyond the storm tracks (note that precipitation nearly halves
404 poleward of approximately 75°; compare Figs. 1c and 5c). To a certain extent RESS can be expected
405 to decrease because of less precipitation formation. But the larger picture requires consideration
406 of the steady-state changes. Change in RH with the RHc100 setup is depicted in Fig. 5d. RH is
407 significantly increased in regions where cloud formation at less than 100% RH had kept WV from
408 being transported. Thus, more WV is isentropically transported to the polar upper troposphere
409 before clouds are formed. This increase in RH, combined with decreased precipitation, results in
410 weakened RESS, especially in the extratropics where the increase in RH is most significant. Less
411 precipitation falling through moister air leads to weaker RESS.

412 In addition to an increase in RH, with the RHc100 setup, CF is significantly amplified in the polar
413 extratropics as the peaks shift poleward (Fig. 5e). With seemingly more difficult conditions for
414 cloud formation, CF increases everywhere (above 850 hPa). This can be understood by considering
415 what triggers cloud formation in the cloud scheme: high values of RH. The increase in average RH
416 noted previously does in fact correspond to a rise in occurrences of high RH as shown through a
417 histogram of daily RH values (Fig. 5g) where values in the [100%, 105%] bin increase drastically,
418 but all other values decrease slightly. A histogram of daily CF values (Fig. 5h) shows a decrease
419 in CF values below 65% and a drastic rise in occurrences of the highest values with the final
420 bin being the highest populated. (Note that while RH values greater than 100% are possible, by
421 definition, 100% is the maximum possible CF value such that the final CF histogram bin represents
422 values of exactly 100% CF.) With 100% grid-mean RH required for cloud formation, when cloud

423 formation is triggered it must be 100% CF at the time-step of the model. These histograms were
424 further broken down by meridional and vertical flow direction (not shown). Poleward and upward
425 flows accounted for the highest RH values and thus the higher CF values, but overall the stratified
426 histograms painted the same picture. For every direction of flow, the RHc100 perturbation requires
427 greater RH for cloud formation, increasing high RH values and thus CF.

428 While CF increases significantly, the change in CC in the free troposphere is small, and in most
429 places is a decrease as seen in Fig. 5f. (A significant loss of CC below 850 hPa not shown is a
430 result of the region being generally unsaturated, since surface evaporation is associated with a time
431 scale.) While changes in CF and CC need not totally align, such drastic differences are surprising
432 and are, in fact, largely an artifact of altering the macrophysics in a way that is unexpected by
433 the microphysics scheme. With the RHc100 condition, if clouds form in a grid cell, the grid cell
434 CF is 100%. Yet with higher CF, autoconversion decreases. In the microphysics scheme, the rate
435 of change of cloud liquid due to autoconversion is proportional to $CF * (LCC/CF)^{(7/3)}$ or, in a
436 frequently-invoked limiter, $\ln(LCC/CF) * LCC$ (see Rotstayn 1997). In other words, if CC is more
437 widely distributed over a higher CF, it triggers less autoconversion. So a rise in CF, unmatched by
438 an increase in CC (since CC is in fact more difficult to form with the RHc100 condition), causes a
439 decrease in autoconversion leading to a cycle slowdown as expected. This result highlights both
440 the non-interchangeability of CC and CF as cloud tracers and the importance of considering the
441 details of a microphysics scheme when evaluating the usefulness of performing drastic alterations.

442 The bigger picture highlighted by the RHc100 case is the significance of isentropic flow and the
443 way in which details of the macrophysics scheme can thus have such significant effects. (Accounting
444 for such phenomena is lacking in advection-condensation theory.) Here, sub-grid-scale RH has
445 a significant effect on extratropical clouds by affecting the storm track locations and altering the
446 frequency of high-RH values. Re-located storm tracks could also have significant effects on

447 shortwave radiation not explored here, contributing to the usefulness of RH_c as a tuning parameter
448 for radiative balance. Thus, the RH_c100 case also emphasizes the additional, non-radiative, impacts
449 of tuning through RH_c , particularly on redistributing WV and precipitation.

450 *c. Sedimentation Perturbations: noRESS*

451 As described previously, one of the most noteworthy differences between saturation adjustment
452 and a full cloud scheme is the addition of two significant sources of WV: rain evaporation and
453 snow sublimation (RESS). As seen in Fig. 1, column-integrated RESS have a significant presence
454 at all latitudes, providing an even stronger source of WV than surface evaporation poleward of
455 approximately 50° . Fig. 2b shows that together they contribute approximately 17% to STET
456 WV sources. RESS defines SE as shown in Fig. 3 with one-fifth of formed precipitation lost to
457 RESS. Fig. 6a depicts the changes in WV tendencies when RESS is no longer present in the Cloud
458 scheme. While surface evaporation increases, the elimination of RESS yields a net decrease in WV
459 sources (Fig. 2d). Matching this decrease, a reduction in LS condensation/deposition (WV sinks)
460 is spatially correlated both latitudinally and vertically with the eliminated RESS. Thus, as in the
461 RH_c100 case, WV and CC cycling is weakened: the total WV/CC sources or sinks in noRESS are
462 13-16% less than in the Cloud case, while still greater than in the Base case (see Fig. 2). However,
463 at the same time, the residence time of a water molecule in the atmosphere is decreased by 7% due
464 to the elimination of RESS as WV sources which come from recycled hydrometeors.

465 Without RESS as sinks of precipitation, STET precipitation increases by $\sim 5\%$ (8% globally)
466 as seen in Fig. 6c and Table 2. By definition, without RESS, SE is 100%. As FE is nearly
467 unchanged, PE increases drastically from 78.3% to 97.9% with a moderate increase in precipitation.
468 The elimination of snow sublimation corresponds strongly with the pattern and magnitude of a
469 decrease in ice settling yielding only a slight change in precipitation poleward of 45° . However, in

470 the subtropics, the elimination of rain evaporation is unmatched by decreases in autoconversion and
471 accretion, so the precipitation increase is mostly subtropical, while the storm tracks are virtually
472 unaffected.

473 This feature can be rationalized by considering the location of WV sources and sinks and
474 the connection between these budgetary terms and the steady-state fields. From a steady-state
475 perspective, the role of RESS in redistributing WV and moistening the atmosphere can be seen
476 in Fig. 6d. Turning off RESS results in a significant decrease in RH (up to 6%), especially in the
477 subtropics and the polar lower troposphere. Additional experiments were performed with RESS
478 turned off locally, including only between 15° and 45° or elsewhere (not shown). These runs
479 resulted in RH being only reduced (with any significance) in the regions where RESS is turned
480 off, demonstrating the local nature of the contribution of RESS to moisture. In redistributing
481 WV, RESS also plays a significant role in the cloud distribution. Without RESS, both CF and CC
482 decrease globally as shown in Fig. 6e-f. The change in CF is of a similar pattern to the change in RH
483 in the polar extratropics, while the change in CC is more concentrated in the storm tracks (where CC
484 is larger to begin with). RH and CF changes are directly connected, as confirmed by considering
485 histograms of extratropical RH and CF (Fig. 6g-h). The noRESS case shifts occurrences of
486 RH away from higher values (>95%) in the extratropical free troposphere corresponding with a
487 decrease in CF concentrated where RH values are highest to begin with.

488 The connection between budgetary and steady-state changes is nuanced. Globally, the general
489 reduction in RH is to be expected since the lack of RESS results in a drying of the boundary
490 layer. This drying triggers more surface evaporation, but no others sources of WV. Decreased
491 higher values of RH leads to decreased clouds. But, spatially, the areas of largest RH change
492 (free troposphere, especially the polar extratropics) do not coincide with the locations of largest
493 RESS tendency. RESS provides a significant source of WV throughout the boundary layer and

494 free troposphere, especially in the tropics (not shown). However, while RESS is smallest in the
495 extratropics, its relative importance as a source of WV is greatest there (see Fig. 1a). While surface
496 evaporation can easily increase below 850 hPa to replace RESS as a source of WV in the boundary
497 layer (which is always nearly saturated), its ability to replenish moisture above 850 hPa depends
498 on circulation. The rising motions induced by the Hadley circulation in the tropics allow humidity
499 (and thus clouds) to be less affected by the loss of RESS. In contrast, in the polar regions where
500 less vertical motion takes place and horizontal transport is more important for WV, the lower
501 troposphere above 850 hPa experiences significant drying. From an isentropic perspective, the
502 drier extratropics can be thought of as the result of less moisture being supplied to the mid-latitude
503 eddies so that less WV is condensed near the poles. The decrease in LS condensation is consistent
504 with a smaller isentropic WV gradient.

505 Thus, in the storm tracks and high latitudes, the increase in precipitation is small since the
506 elimination of RESS dries the region creating two opposing effects. Precipitation is increased
507 since SE is now 100%, but this increase is nearly balanced by a reduction in precipitation due to
508 less moisture and thus fewer precipitating clouds in the region. However, in the subtropics and mid
509 latitudes, the direct increase in precipitation is largely unbalanced since clouds are less affected
510 (as clouds are few to begin with so humidity decreases have little effect). This local role of RESS
511 is further seen in the fact that P-E (Fig. 6c) remains largely unchanged. Ultimately, the role of
512 RESS in the free troposphere is to increase RH (and ultimately clouds) by providing an additional
513 source of WV, while decreasing precipitation and—to a much greater extent—the PE through the
514 introduction of an atmospheric sink for hydrometeors.

515 *d. Formation Perturbation: halvAUTO*

516 In the halvAUTO case, autoconversion decreases in the STET region by 29%. Accretion and
517 ice settling increase by 19% and 4%, respectively, to keep total STET CC sinks only 3% less than
518 in the Cloud case. Similarly, in the doubAUTO case, STET autoconversion increases by 34%,
519 accretion decreases by 22%, and ice settling increases by 6%, such that total CC sinks are only 3%
520 more than in the Cloud case. These changes can be seen in Fig. 2e and f. In both cases the relative
521 balances of the WV sources and sinks is roughly unchanged with a slight re-balancing of RESS
522 as snow increases with a decrease of rain in halvAUTO and vice versa in doubAUTO. Noting the
523 parallel opposing changes in halvAUTO and doubAUTO, we focus primarily on halvAUTO.

524 Fig. 7a shows that latitudinally the WV balance is unchanged with decreases in LS condensation,
525 surface evaporation, and rain evaporation balancing each other. Similarly, the CC balance (Fig. 7b)
526 stays latitudinally unchanged with a decrease in LS condensation balanced by the net decreases
527 in CC sinks. The opposing changes in autoconversion and accretion are similar in their spatial
528 pattern, but the decrease in autoconversion is stronger, resulting in less precipitation as shown in
529 Fig. 7c. These changes are principally equatorward of 60° since that is where autoconversion is
530 most significant in the first place (Fig. 1b).

531 Across the STET region, precipitation decreases in the halvAUTO case by 3% and increases in
532 the doubAUTO case by 4%, similar to how the strength of the WV/CC cycle changes. From an
533 efficiency perspective (see Table 2), CE and FE change slightly in the same direction as changes
534 in precipitation, decreasing in halvAUTO in line with a cycle slowdown. SE also changes slightly
535 but in the opposite way: with decreased net formation but a proportionally larger decrease in
536 RESS in the halvAUTO case, SE increases slightly. The FE and SE effects balance such that PE
537 is minimally affected. This finding holds true for smaller and larger alterations to autoconversion,

538 accretion, and N except when an artificial decrease in a process is so large that the other processes
539 cannot keep the WV/CC cycle roughly constant. For example, when autoconversion is completely
540 eliminated, total STET CC sinks decrease by 6% as accretion cannot come close to making up for
541 the difference reducing FE to 90.4% and PE to 72.1%. However, apart from such limiting cases,
542 changes in budgetary terms and efficiencies are roughly linear. The residence time increases with
543 halvAUTO with weakened precipitation since a water molecule now spends a longer time in the
544 atmosphere as CC before precipitating, while the doubAUTO case shows a corresponding decrease
545 in residence time.

546 From a steady-state perspective, in the halvAUTO case, RH, CF, and CC all increase as shown in
547 Fig. 7d-f. The significant changes are spatially similar, concentrated equatorward of 60° (where the
548 net decrease in CC sinks was strongest) and below ~ 500 hPa, peaking in the storm tracks. These
549 steady-state changes described are qualitatively opposite in the doubAUTO case (not shown). Of
550 note, the steady-state RH and cloud fields change not in response to a shift in the balance between
551 autoconversion and accretion, but in response to changes in total sources/sinks. When WV/CC
552 cycling strengthened due to increased autoconversion, increased accretion, or decreased N , an
553 amplification of RH, CF, and CC resulted. Opposite changes are associated with WV/CC cycling
554 weakening. Re-balancing autoconversion and accretion must have a relatively innocuous effect on
555 RH and clouds in and of itself.

556 Why does a strengthened (weakened) cycle increase (decrease) RH and clouds? It is important to
557 note that this generalization does not extend past these perturbations. (The pattern is followed in the
558 RHc100 case discussed previously but not in the noRESS case, possibly because of the significant
559 spatial and physical differences resulting from replacing RESS as WV sources with enhanced
560 surface evaporation.) However, in the absence of other changes, a longer (shorter) residence time
561 for a water molecule in the atmosphere could be expected to correspond to an increase (decrease)

562 in the steady-state fields which represent the forms that a water molecule takes as it resides in
563 the atmosphere. Additionally, steady-state RH is directly connected to the WV cycle through
564 surface evaporation since it is formulated as a function of subsaturation. RH is connected to CF
565 as demonstrated by considering histograms of RH and CF (Fig. 7): the halvAUTO case slightly
566 shifts occurrences of RH toward the highest values ($>100\%$). Without any significant changes
567 to the cloud physics beyond a re-balancing of autoconversion and accretion, CC can logically be
568 expected to follow CF.

569 Thus, the formation perturbations demonstrate the resilience of this cloud microphysics scheme
570 to changes in the balance of formation tendencies in terms of PE. Additionally, the general patterns
571 for steady-state consequences of the WV/CC cycle weakening (strengthening) emerge showing how
572 steady-state fields are affected by changes in residence time. A weakened (strengthened) cycle,
573 apart from other changes in cloud physics, leads to an increased (decreased) residence time and
574 diminished (amplified) steady-state RH, CC, and CF.

575 **4. Discussion and Conclusions**

576 *a. Summary*

577 The general picture that emerges from this idealized modeling study is that circulation sets the
578 basic pattern of moisture and precipitation, as seen through the first order similarity between the two
579 control cases. In the perturbation runs, details of the physics of condensation and sedimentation
580 also have substantial effects on humidity, clouds, and precipitation. However, it is noteworthy
581 that while RH does differ significantly between the control cases, precipitation does not, as the
582 precipitation changes in the condensation and sedimentation perturbations (RHc100 and noRESS)
583 are of opposing sign. A secondary picture is the utility of this idealized GCM for understanding

584 physical controls of free tropospheric clouds and responses to perturbations since key processes
585 can be cleanly isolated. The saturation adjustment scheme (Base case) shows gross RH features, as
586 expected from advection-condensation theory, but cloud processes refine the features. In particular,
587 cloud macrophysics are important since thresholds for cloud formation change cloud distribution
588 (including the CF/CC ratio) and hence RH due to isentropic transport of moisture as shown in
589 the RHc100 run. Cloud microphysics are equally important, adding a key component through
590 the re-evaporation of hydrometeors (RESS) changing RH values by a similar magnitude, as much
591 as 5-6%. However, the formation perturbations demonstrate that the balance of precipitation-
592 forming processes (here autoconversion and accretion) have little significance for RH, cloudiness,
593 precipitation, and especially PE.

594 *b. Advection-Condensation Theory*

595 As was discussed previously, there are, on the surface, three differences between a saturation
596 adjustment scheme (or advection-condensation theory) and a full cloud scheme: RH_c , RESS, and
597 presence of CC which can be advected and/or subject to LS evaporation/sublimation. The first
598 two differences are here individually directly removed, but the third must be explored as a residual
599 in the *RHc100_noRESS* experiment where we remove the RH_c and RESS effects together from
600 the Cloud case. If these three identified differences are exhaustive, RHc100_noRESS represents
601 the effect of adding CC to the Base case. Additionally, if the RH_c and RESS effects are linearly
602 additive, we can mathematically manipulate the various experiments to isolate the separate effects
603 of RH_c and RESS added to the Base case (as opposed to removing these effects from the Cloud case
604 as was described in the Results section). To this end, Fig. 8 explores to what extent the RH_c and
605 RESS effects are linearly additive, to what extent they can explain the full difference between the

606 Base and Cloud controls, and the characteristics of the residual differences which can be attributed
607 to CC advection.

608 The RHc100 run includes RESS and advection effects, the noRESS run includes RHc and
609 advection effects, and the RHc100_noRESS run is just the advection effect. So we can test for
610 linearity of the RH_c and RESS effects by comparing RHc100 plus noRESS minus RHc100_noRESS
611 (Fig. 8a). The combination appears to be mostly linear except in the free tropospheric high latitudes
612 where both RHc100 and noRESS runs had significant, but opposing, effects. RHc100 leads to
613 moistening and noRESS to drying; linear addition over-emphasizes drying or under-emphasizes
614 moistening. A possible mechanism is that when both are implemented, there is less moisture (from
615 noRESS) to be exported to the high latitudes (in RHc100), but this effect should be minimal as
616 noRESS minimally dries the boundary layer. A more like explanation is that since in RHc100,
617 RESS decreases by over 50%, the noRESS drying effect is dampened when combined. But since
618 they combine nearly linearly, we can separately analyze the three effects of adding a cloud scheme
619 to a saturation adjustment scheme.

620 When adding a cloud scheme to a saturation adjustment scheme, advection and LS evapora-
621 tion/sublimation (and any other residual effects, for example, nucleation barrier and incomplete
622 fallout in cirrus as noted by Liu et al. (2010)) moistens the free tropospheric subtropics and mid-
623 latitudes (Fig. 8b) as well as the polar stratosphere. Implementing a RH_c of 83.3% dries the high
624 latitudes (Fig. 8c) by allowing for more condensation and precipitation of moisture before it is
625 isentropically transported to the poles. Finally RESS moistens the free troposphere, most strongly
626 in the storm tracks and lower polar regions (Fig. 8d), by adding an additional source of WV above
627 the boundary layer.

628 Thus, this work highlights the key deficiencies with an advection-condensation paradigm. The
629 relatively small residual effects seen when comparing RHc100_noRESS minus Base to Cloud

630 minus base (Fig. 8b) suggest that RH_c and RESS are the key ways in which a cloud scheme alters
631 the RH distribution from advection-condensation theory alone, in the absence of cloud processes
632 altering the circulation through latent heat release or cloud radiative effects. RESS is a cloud micro-
633 physical effect already noted as missing from the advection-condensation paradigm and important
634 to moistening the subtropics. But here we also highlight its important for moistening the polar
635 regions where less vertical motion makes surface evaporation less effective at moistening the free
636 troposphere. In contrast, RH_c is a macrophysical effect, an artifact of parameterizations attempting
637 to represent the RH variability present in the real world. Here we emphasize the importance of
638 considering sub-grid-scale humidity distribution to allow clouds to form in appropriate latitudinal
639 locations. As Sherwood et al. (2010) noted, these components of why the advection-condensation
640 is inadequate are critical to understand in order to accurately model not just climatological values,
641 but importantly changes in RH (and hence clouds and precipitation) with warming.

642 *c. Outlook*

643 The picture presented here is likely to change significantly with warming. While the advection-
644 condensation paradigm suggests that free tropospheric RH is unlikely to change significantly with
645 uniform warming (Sherwood et al. 2010), the specific deficiencies of advection-condensation
646 theory explored here confound predicting changes in RH with warming, already complicated by
647 non-uniform warming. Any changes in RH could also have implications for P-E changes, as the
648 wet-get-wetter paradigm (Held and Soden 2006) is predicated on unchanged lower-tropospheric RH
649 and flow. Sherwood et al. (2014) identified a mixing-induced low cloud feedback where enhanced
650 mixing with warming dehydrates the boundary layer. Here, as in advection-condensation theory,
651 we highlighted the connection between subtropical boundary layer humidity and polar upper
652 tropospheric humidity because of eddy isentropic transport. In addition to the complications of

653 dynamical effects, because of the Clausius-Clapeyron relation, WV transport is expected to increase
654 with warming for thermodynamic reasons (Lavers et al. 2015). And as noted in the introduction,
655 replacement of ice with liquid in mixed-phase clouds with warming may also effect moisture and
656 cloud distribution through changes in precipitation efficiency. Thus, modeling the mechanisms
657 controlling extratropical humidity and clouds accurately is critical for confidently forecasting future
658 change.

659 Our perturbation results demonstrate the significance of key processes for defining steady-state
660 patterns of humidity and cloudiness, implying a strong need to constrain processes such as RESS and
661 sub-grid-scale RH in order to ensure the physical grounding of parameterizations so that responses
662 to altered forcings will also be physical. Additionally, while *accr/auto* (or *N*) was not important
663 here in terms of affecting steady-state fields or average precipitation, it is likely to have other effects
664 as discussed in the introduction, including modulating the intensity of precipitation events. Our
665 results suggest that the strength of warm rain processes as a whole (accretion+autoconversion) plays
666 a role in defining RH, clouds, and precipitation distribution and thus is an important parameter
667 to constrain, not just *accr/auto*. By separately analyzing the effects on CF and CC and their
668 connection to changes in RH and various components of the water cycle, this study highlighted the
669 need to carefully dissect the physical mechanisms for change instead of relying on generalizations.
670 For example, as demonstrated in the RHc100 perturbation, cloud response cannot be directly
671 predicted from changes in average RH.

672 Comparing the significance of various controls of clouds cannot be precise in this idealized,
673 decoupled framework. Nor does this study explore the relative significance of various cloud
674 feedbacks to anthropogenic forcings. Yet, by allowing for a detailed exploration of cloud physics
675 decoupled from circulation, this type of idealized model could play a key role in the model
676 hierarchy for reducing uncertainty surrounding cloud feedback. In comprehensive GCMs with

677 coupled feedbacks, circulation feedbacks (particularly shifts in the extratropical jets) have been
678 demonstrated to be less significant than thermodynamic mechanisms of mixed-phase clouds in
679 creating the shortwave extratropical cloud feedback (Wall and Hartmann 2015; Ceppi and Hartmann
680 2016). This finding suggests that cloud parameterization mechanisms relating to mixed-phase
681 clouds may play a significant role in constraining extratropical cloudiness, an area explored in
682 related work with the idealized setup used in this paper (?).

683 In summary, this study takes a step forward in elucidating physical mechanisms controlling
684 extratropical clouds, while highlighting the importance of identifying and adequately representing
685 these mechanisms in order to accurately simulate the cloud feedbacks associated with climate
686 change.

687 *Acknowledgments.* The authors acknowledge

688 M.E.F. was supported by award NA18OAR4320123 from the National Oceanic and Atmospheric
689 Administration, U.S. Department of Commerce, and award AWD1005319 from the National
690 Science Foundation.

691 *Data availability statement.* The output from the simulations described in this manuscript is
692 archived at the Geophysical Fluid Dynamics Laboratory and is available upon request.

693 **References**

694 Bony, S., and Coauthors, 2015: Clouds, circulation and climate sensitivity. *Nat. Geosci.*, **8**, 261–
695 268, doi:10.1038/ngeo2398.

696 Ceppi, P., F. Briant, M. D. Zelinka, and D. L. Hartmann, 2017: Cloud feedback mechanisms and
697 their representation in global climate models. *WIREs Clim. Change*, **8**, doi:10.1002/wcc.465.

- 698 Ceppi, P., and D. L. Hartmann, 2016: Clouds and the atmospheric circulation response to warming.
699 *J. Climate*, **29**, 783–799, doi:10.1175/JCLI-D-15-0394.1.
- 700 Ceppi, P., D. L. Hartmann, and M. J. Webb, 2016: Mechanisms of the negative shortwave cloud
701 feedback in middle to high latitudes. *J. Climate*, **29**, 139–157, doi:10.1175/JCLI-D-15-0327.1.
- 702 Frierson, D. M. W., I. M. Held, and P. Zurita-Gotor, 2006: A gray-radiation aquaplanet moist GCM.
703 Part I: Static stability and eddy scale. *J. Atmos. Sci.*, **63**, 2548–2566, doi:10.1175/JAS3753.1.
- 704 Galewsky, J., A. Sobel, and I. M. Held, 2005: Diagnosis of subtropical humidity dynamics using
705 tracers of last saturation. *J. Atmos. Sci.*, **62**, 3353–3367, doi:10.1175/JAS3533.1.
- 706 Geoffroy, O., S. C. Sherwood, and D. Fuchs, 2017: On the role of the stratiform cloud scheme
707 in the inter-model spread of cloud feedback. *J. Adv. Model. Earth Syst.*, **9**, 423–437, doi:
708 10.1002/2016MS000846.
- 709 Gettelman, A., H. Morrison, C. R. Terai, and R. Wood, 2013: Microphysical process rates
710 and global aerosol-cloud interactions. *Atmos. Chem. Phys.*, **13**, 9855–9867, doi:10.5194/
711 acp-13-9855-2013.
- 712 Gettelman, A., H. Morrison, C. R. Terai, and R. Wood, 2014: Corrigendum to "Microphysical
713 process rates and global aerosol-cloud interactions". *Atmos. Chem. Phys.*, **14**, 9099–9103, doi:
714 10.5194/acp-14-9099-2014.
- 715 Held, I. M., 2005: The gap between simulation and understanding in climate modeling. *Bull. Amer.*
716 *Meteor. Soc.*, **86**, 1609–1614, doi:10.1175/BAMS-86-11-1609.
- 717 Held, I. M., 2014: Simplicity amid complexity. *Science*, **343**, 1206–1207, doi:10.1126/science.
718 1248447.

- 719 Held, I. M., and T. Schneider, 1999: The surface branch of the zonally averaged mass transport
720 circulation in the troposphere. *J. Atmos. Sci.*, **56**, 1688–1697, doi:10.1175/1520-0469(1999)
721 056<1688:TSBOTZ>2.0.CO;2.
- 722 Held, I. M., and B. J. Soden, 2006: Robust responses of the hydrological cycle to global warming.
723 *J. Climate*, **19**, 5686–5699, doi:10.1175/JCLI3990.1.
- 724 Held, I. M., and M. J. Suarez, 1994: A proposal for the intercomparison of the dynamical
725 cores of atmospheric general circulation models. *Bull. Amer. Meteor. Soc.*, **75**, 1825–1830,
726 doi:10.1175/1520-0477(1994)075<1825:APFTIO>2.0.CO;2.
- 727 Jeevanjee, N., P. Hassanzadeh, S. Hill, and A. Sheshadri, 2017: A perspective on climate model
728 hierarchies. *J. Adv. Model. Earth Syst.*, **9**, 1760–1771, doi:10.1002/2017MS001038.
- 729 Jiang, H., G. Feingold, and A. Sorooshian, 2010: Effect of aerosol on the susceptibility and
730 efficiency of precipitation in warm trade cumulus clouds. *J. Atmos. Sci.*, **67**, 3525–3540, doi:
731 10.1175/2010JAS3484.1.
- 732 Jing, X., K. Suzuki, H. Guo, D. Goto, T. Ogura, T. Koshiro, and J. Mülmenstädt, 2017: A multi-
733 model study on warm precipitation biases in global models compared to satellite observations.
734 *J. Geophys. Res. Atmos.*, **122**, 11 806–11 824, doi:10.1002/2017JD027310.
- 735 Kelly, K., A. Tuck, and T. Davies, 1991: Wintertime asymmetry of upper tropospheric water
736 between the Northern and Southern Hemispheres. *Nature*, **353**, 244–247, doi:10.1038/353244a0.
- 737 Klein, S. A., and Coauthors, 2009: Intercomparison of model simulations of mixed-phase clouds
738 observed during the ARM Mixed-Phase Arctic Cloud Experiment. I: Single-layer cloud. *Quart.*
739 *J. Roy. Meteor. Soc.*, **135**, 979–1002, doi:10.1002/qj.416.

- 740 Laliberté, F., T. Shaw, and O. Pauluis, 2012: Moist recirculation and water vapor transport on dry
741 isentropes. *J. Atmos. Sci.*, **69**, 875–890, doi:10.1175/JAS-D-11-0124.1.
- 742 Langhans, W., K. Yeo, and D. M. Romps, 2015: Lagrangian investigation of the precipitation
743 efficiency of convective clouds. *J. Atmos. Sci.*, **72**, 1045–1062, doi:10.1175/JAS-D-14-0159.1.
- 744 Lavers, D. A., F. M. Ralph, D. E. Waliser, A. Gershunov, and M. D. Dettinger, 2015: Climate
745 change intensification of horizontal water vapor transport in CMIP5. *Geophys. Res. Lett.*, **42**,
746 5617–5625, doi:10.1002/2015GL064672.
- 747 Liu, Y. S., S. Fueglistaler, and P. H. Haynes, 2010: Advection-condensation paradigm for strato-
748 spheric water vapor. *J. Geophys. Res. Atmos.*, **115**, D24 307, doi:10.1029/2010JD014352.
- 749 McCoy, D. T., D. L. Hartmann, and M. D. Zelinka, 2018: Mixed-phase cloud feedbacks. *Mixed-
750 Phase Clouds: Observations and Modeling*, C. Andronache, Ed., Elsevier, 215–236, doi:10.
751 1016/B978-0-12-810549-8.00009-X.
- 752 McCoy, D. T., D. L. Hartmann, M. D. Zelinka, P. Ceppi, and D. P. Grosvenor, 2015: Mixed-phase
753 cloud physics and Southern Ocean cloud feedback in climate models. *J. Geophys. Res. Atmos.*,
754 **120**, 9539–9554, doi:10.1002/2015JD023603.
- 755 McCoy, D. T., I. Tan, D. L. Hartmann, M. D. Zelinka, and T. Storelvmo, 2016: On the relationships
756 among cloud cover, mixed-phase partitioning, and planetary albedo in GCMs. *J. Adv. Model.
757 Earth Syst.*, **8**, 650–668, doi:10.1002/2015MS000589.
- 758 Michibata, T., and T. Takemura, 2015: Evaluation of autoconversion schemes in a single model
759 framework with satellite observations. *J. Geophys. Res. Atmos.*, **120**, 9570–9590, doi:10.1002/
760 2015JD023818.

- 761 Ming, Y., and I. M. Held, 2018: Modeling water vapor and clouds as passive tracers in an idealized
762 GCM. *J. Climate*, **31**, 775–786, doi:10.1175/JCLI-D-16-0812.1.
- 763 Pierrehumbert, R. T., 1998: Lateral mixing as a source of subtropical water vapor. *Geophys. Res.*
764 *Lett.*, **25**, 151–154, doi:10.1029/97GL03563.
- 765 Pierrehumbert, R. T., H. Brogniez, and R. Roca, 2007: On the relative humidity of the atmosphere.
766 *The Global Circulation of the Atmosphere*, T. Schneider, and A. H. Sobel, Eds., Princeton
767 University Press, 143–185.
- 768 Quaas, J., and Coauthors, 2020: Constraining the Twomey effect from satellite observations: issues
769 and perspectives. *Atmos. Chem. Phys.*, **20**, 15 079–15 099, doi:10.5194/acp-20-15079-2020.
- 770 Rotstajn, L. D., 1997: A physically based scheme for the treatment of stratiform clouds and
771 precipitation in large-scale models. I: Description and evaluation of the microphysical processes.
772 *Q. J. R. Meteorol. Soc.*, **123**, 1227–1282.
- 773 Rotstajn, L. D., B. F. Ryan, and J. J. Katzfey, 2000: A scheme for calculation of the liquid fraction
774 in mixed-phase clouds in large-scale models. *Mon. Wea. Rev.*, **128**, 1070–1088.
- 775 Shepherd, T. G., 2014: Atmospheric circulation as a source of uncertainty in climate change
776 projections. *Nat. Geosci.*, **7**, 703–708, doi:10.1038/ngeo2253.
- 777 Sherwood, S., S. Bony, and J.-L. Dufresne, 2014: Spread in model climate sensitivity traced to
778 atmospheric convective mixing. *Nature*, **505**, 37–42, doi:10.1038/nature12829.
- 779 Sherwood, S. C., R. Roca, T. M. Weckwerth, and N. G. Andronova, 2010: Tropospheric water
780 vapor, convection, and climate. *Rev. Geophys.*, **48**, doi:10.1029/2009RG000301.
- 781 Sherwood, S. C., and Coauthors, 2020: An assessment of Earth’s climate sensitivity using multiple
782 lines of evidence. *Reviews of Geophysics*, **58**, e2019RG000 678, doi:10.1029/2019RG000678.

- 783 Stephens, G. L., 1978: Radiation profiles in extended water clouds. II. Parameterization schemes.
784 *J. Atmos. Sci.*, **35**, 2123–2132, doi:10.1175/1520-0469(1978)035<2123:RPIEWC>2.0.CO;2.
- 785 Stevens, B., and S. Bony, 2013: What are climate models missing? *Science*, **340**, 1053–1054,
786 doi:10.1126/science.1237554.
- 787 Sun, D.-Z., and R. S. Lindzen, 1993: Distribution of tropical tropospheric water vapors. *J. Atmos.*
788 *Sci.*, **50**, 1643–1660, doi:10.1175/1520-0469(1993)050<1643:DOTTWV>2.0.CO;2.
- 789 Trenberth, K. E., 1998: Atmospheric moisture residence times and cycling: Implications for
790 rainfall rates and climate change. *Climatic Change*, **39**, 667–694.
- 791 Wall, C. J., and D. L. Hartmann, 2015: On the influence of poleward jet shift on shortwave cloud
792 feedback in global climate models. *J. Adv. Model. Earth Syst.*, **7**, doi:10.1002/2015MS000520.
- 793 Wu, P., B. Xi, X. Dong, and Z. Zhang, 2018: Evaluation of autoconversion and accre-
794 tion enhancement factors in general circulation model warm-rain parameterizations using
795 ground-based measurements over the Azores. *Atmos. Chem. Phys.*, **18**, 17 405–17 420, doi:
796 10.5194/acp-18-17405-2018.
- 797 Yang, H., and R. T. Pierrehumbert, 1994: Production of dry air by isentropic mixing. *J. Atmos.*
798 *Sci.*, **51**, 3437–3454, doi:0.1175/1520-0469(1994)051<3437:PODABI>2.0.CO;2.
- 799 Zhao, M., 2014: An investigation of the connections among convection, clouds, and climate
800 sensitivity in a global climate model. *J. Climate*, **27**, 1845–1862, doi:10.1175/JCLI-D-13-00145.
801 1.
- 802 Zhao, M., I. M. Held, S.-J. Lin, and G. A. Vecchi, 2009: Simulations of global hurricane climatol-
803 ogy, interannual variability, and response to global warming using a 50-km resolution GCM. *J.*
804 *Climate*, **22**, 6653–6678, doi:10.1175/2009JCLI3049.1.

805 **LIST OF TABLES**

806 **Table 1.** Description of the experiments. 38

807 **Table 2.** Summary of STET (15°-90°) precipitation variables: average precipitation (P)
808 and evaporation (E); condensation (CE), formation (FE), sedimentation (SE),
809 and precipitation (PE) efficiencies; residence time (RT). See text for definition
810 of these variables. 39

TABLE 1. Description of the experiments.

Name	Description
Base	control simulation with specific humidity tracer and saturation adjustment
Cloud	control simulation with specific humidity and cloud tracers (liquid, ice, and fraction) and microphysics
RHc100	variant of Cloud simulation requiring 100% grid-box-mean RH for cloud formation (RH_c)
noRESS	variant of Cloud simulation without rain evaporation or snow sublimation
halvAUTO	variant of Cloud simulation halving the raw computed value for autoconversion at each time-step
doubAUTO	as halvAUTO, but doubling, instead of halving, autoconversion
RHc100_noRESS	variant of Cloud simulation combining both RHc100 and noRESS variations

811 TABLE 2. Summary of STET (15°-90°) precipitation variables: average precipitation (P) and evaporation (E);
 812 condensation (CE), formation (FE), sedimentation (SE), and precipitation (PE) efficiencies; residence time (RT).
 813 See text for definition of these variables.

run	P	E	CE	FE	SE	PE	RT
	mm day ⁻¹		%				days
Base	1.84	2.34	78.5	–	–	–	13.1
Cloud	1.91	2.37	83.9	98.2	79.7	78.3	12.7
RHc100	1.71	2.17	81.2	95.2	89.4	85.1	14.3
noRESS	2.00	2.47	81.3	97.9	100.	97.9	11.8
halvAUTO	1.84	2.31	83.6	97.6	79.8	77.9	13.1
doubAUTO	1.98	2.44	84.3	98.6	79.6	78.5	12.2

814 **LIST OF FIGURES**

815 **Fig. 1.** Comparison of zonally-averaged, column-integrated WV, CC, and precipitation (P) ten-
816 dency terms in control cases (black totals, blue sources, and red sinks). Cloud case terms
817 (depicted as indicated by the legends) shown are (a) total (WV), surface evaporation (SE),
818 rain evaporation (RE), snow sublimation (SS), and net condensation (Co); (b) total (CC),
819 net condensation (Co), autoconversion (Au), accretion (Ac), and ice settling (IS); (c) total
820 (P), net formation (Form), net sinks (RESS), and moisture convergence (P-E, surface precip-
821 itation minus evaporation). Base case terms (depicted as half-width lines) shown are total
822 WV, surface evaporation, saturation adjustment as net condensation in (a) and precipitation
823 in (c), and saturation adjustment minus evaporation as P-E in (c). Units are $10^{-6} \text{ kg m}^{-2} \text{ s}^{-1}$.
824 A positive tendency value denotes (a) WV, (b) CC, or (c) precipitation increasing. Totals
825 include the less significant tendency terms not shown individually. 42

826 **Fig. 2.** Principal WV and CC sources and sinks for various model runs (see Table 1) represented as
827 column-integrated average STET (15° - 90°) tendency values. For clarity, the smallest terms
828 are conglomerated in an other (O) category. Processes shown are WV sources: surface
829 evaporation (SE), rain evaporation (RE), and snow sublimation (SS); WV sink (CC source):
830 LS condensation (Co); CC sinks: autoconversion (Au), accretion (Ac), and ice settling (IS).
831 Base case saturation adjustment is labeled LS condensation. Tendency units (vertical axis)
832 are $10^{-6} \text{ kg m}^{-2} \text{ s}^{-1}$. Percentages are given with respect to total source or sink category and
833 may not add to 100% due to rounding. 43

834 **Fig. 3.** Diagram of the water cycle in the control cloud microphysics scheme (Cloud experiment).
835 Water is cycled between four species (reservoirs): WV, CC, precipitation, and an assumed
836 surface reservoir. The quantities shown are average STET (15° - 90°) tendency values with
837 units of $10^{-6} \text{ kg m}^{-2} \text{ s}^{-1}$. Each reservoir shows either a balance (0.0) or an imbalance. Here,
838 condensation comprises both LS condensation and deposition; evaporation comprises both
839 LS evaporation and sublimation; formation includes autoconversion, accretion, ice settling,
840 and melting of cloud ice to rain; and sedimentation represents formation processes minus
841 RESS. 44

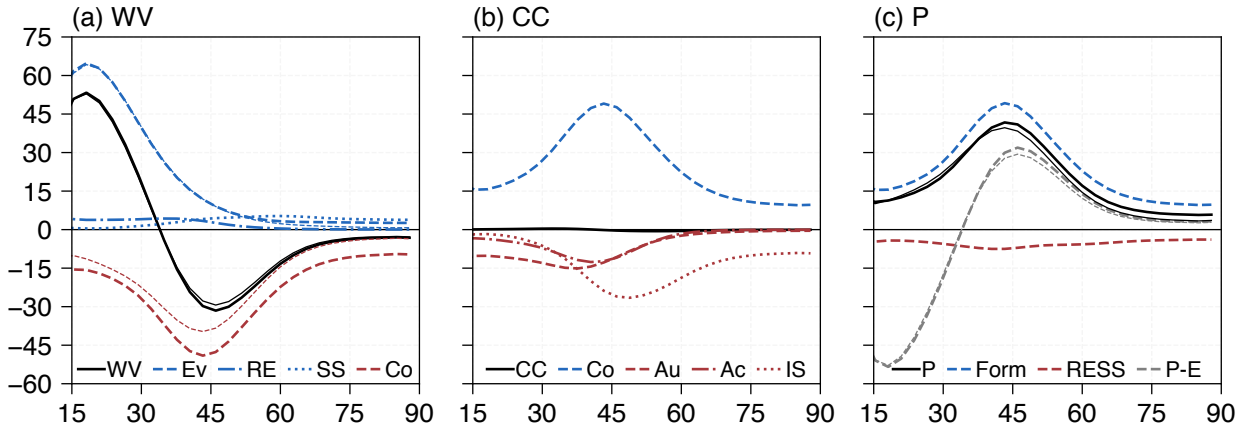
842 **Fig. 4.** Key variables in control runs: (a) RH difference (Cloud minus Base, %) as shading and
843 Base RH as contours (5% spacing), (b) temperature (K) as shading and potential temperature
844 as contours (5K spacing), (c) Cloud CF (%) as shading and Cloud RH as contours (5%
845 spacing), (d) Cloud total CC ($10^{-6} \text{ kg kg}^{-1}$) as shading and liquid (solid) and ice (dashed)
846 CC as contours (5 $10^{-6} \text{ kg kg}^{-1}$ spacing). Variables have been zonally averaged, and the x-
847 and y-axes are latitude and pressure (hPa), respectively. 45

848 **Fig. 5.** Key variable changes in RHc100 perturbation from Cloud control: absolute differences in
849 zonally averaged (a) WV, (b) CC, and (c) precipitation (P) tendency terms (y-axis units of 10^{-6}
850 $\text{kg m}^{-2} \text{ s}^{-1}$); absolute differences in (d) RH, (e) CF, and (f) CC as shading with Cloud values
851 as contours (5%, 5%, and 5 $10^{-6} \text{ kg kg}^{-1}$ spacing, respectively); comparison of normalized
852 histograms of (g) RH and (h) CF in Cloud (black) and RHc100 (grey) cases from daily data
853 (x-axis units of %) between 15° and 90° and 850 and 250 hPa with the y-axis cut off at 0.15.
854 For (a)-(c), WV, CC, and precipitation (P) tendency difference terms shown are as defined
855 in Fig. 1, with units of $10^{-6} \text{ kg m}^{-2} \text{ s}^{-1}$ where a positive tendency difference denotes an
856 increase in a WV/CC/P-increasing process or a decrease in a WV/CC/P-decreasing process.
857 For (a)-(f) variables have been zonally averaged and the x-axis is latitude; for (d-f) the y-axis
858 is pressure (hPa). For (g)-(h), histogram bins have widths of 5% and are all half-open except
859 for the last bin: [0, 5), [5, 10), ..., [100, 105]. 46

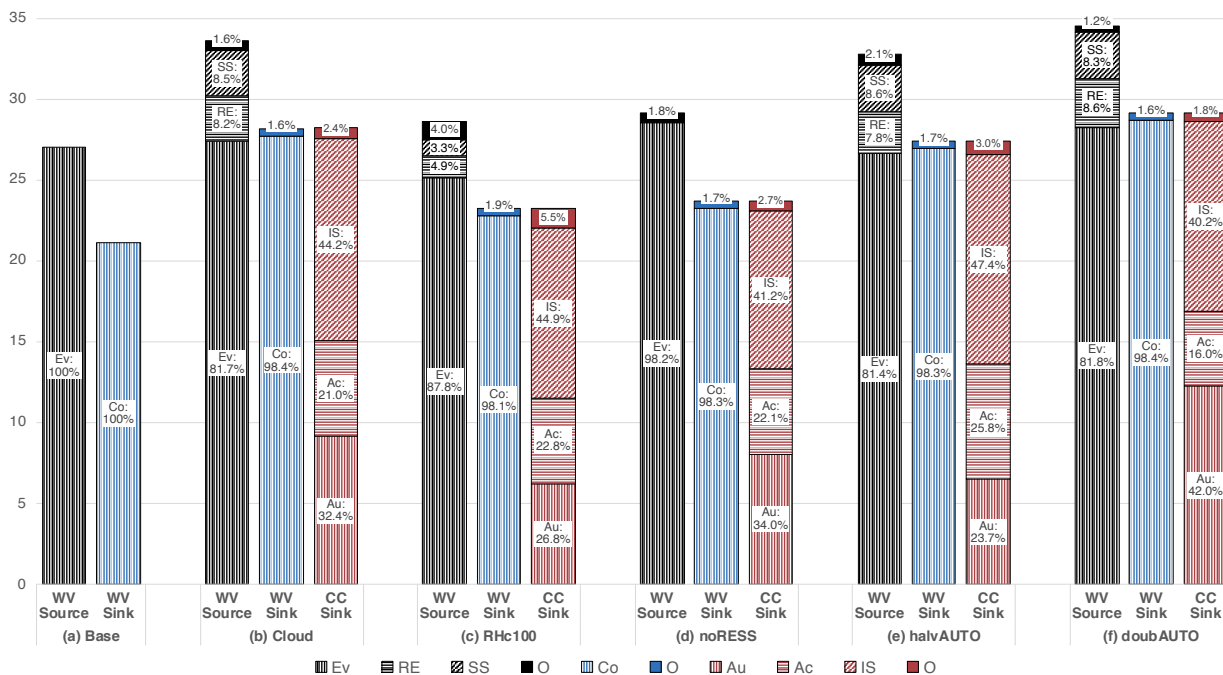
860 **Fig. 6.** As Fig. 5, but for noRESS perturbation. 47

861 **Fig. 7.** As Figs. 5 and 6, but for halvAUTO perturbation, except that the colorbar scale is reduced
862 by a factor of 10 for (d) and (e). 48

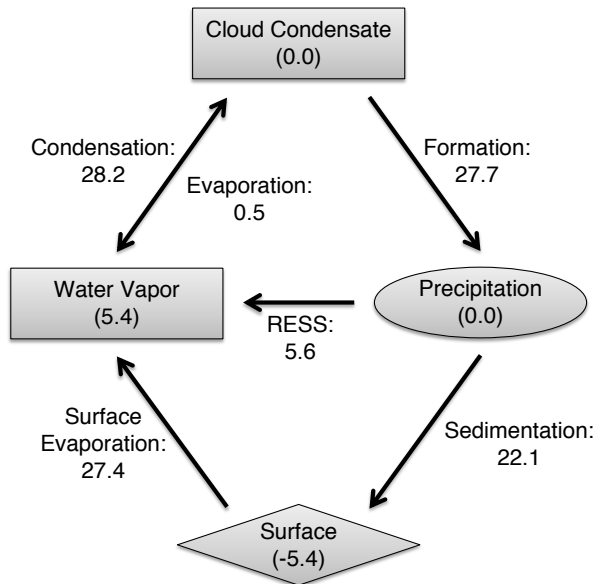
863 **Fig. 8.** Comparison of absolute RH differences (%) between control cases and intermediate setups:
864 (a) RHc100 plus noRESS minus RHc100_noRESS minus Cloud [linearity check: should be
865 0 if $RH_c = 83.3\%$ and RESS effects sum linearly], (b) RHc100_noRESS minus Base [CC
866 advection effect] as shading, (c) noRESS minus RHc100_noRESS [$RH_c = 83.3\%$ effect] as
867 shading, (d) noRESS minus Base [RESS effect] as color shading. All contours are Cloud
868 minus Base difference with a spacing of 1%. 49



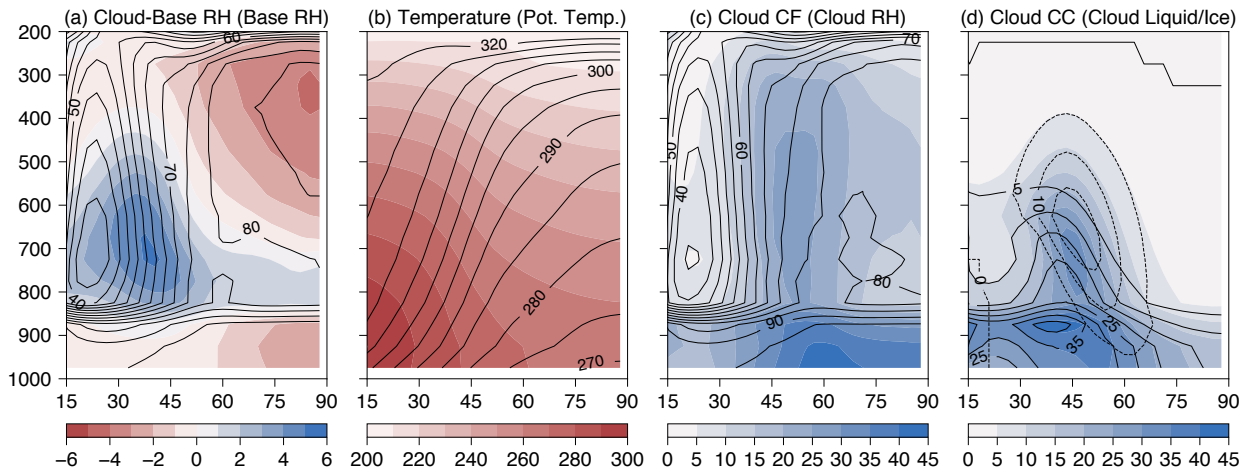
869 FIG. 1. Comparison of zonally-averaged, column-integrated WV, CC, and precipitation (P) tendency terms
 870 in control cases (black totals, blue sources, and red sinks). Cloud case terms (depicted as indicated by the
 871 legends) shown are (a) total (WV), surface evaporation (SE), rain evaporation (RE), snow sublimation (SS),
 872 and net condensation (Co); (b) total (CC), net condensation (Co), autoconversion (Au), accretion (Ac), and
 873 ice settling (IS); (c) total (P), net formation (Form), net sinks (RESS), and moisture convergence (P-E, surface
 874 precipitation minus evaporation). Base case terms (depicted as half-width lines) shown are total WV, surface
 875 evaporation, saturation adjustment as net condensation in (a) and precipitation in (c), and saturation adjustment
 876 minus evaporation as P-E in (c). Units are $10^{-6} \text{ kg m}^{-2} \text{ s}^{-1}$. A positive tendency value denotes (a) WV, (b) CC,
 877 or (c) precipitation increasing. Totals include the less significant tendency terms not shown individually.



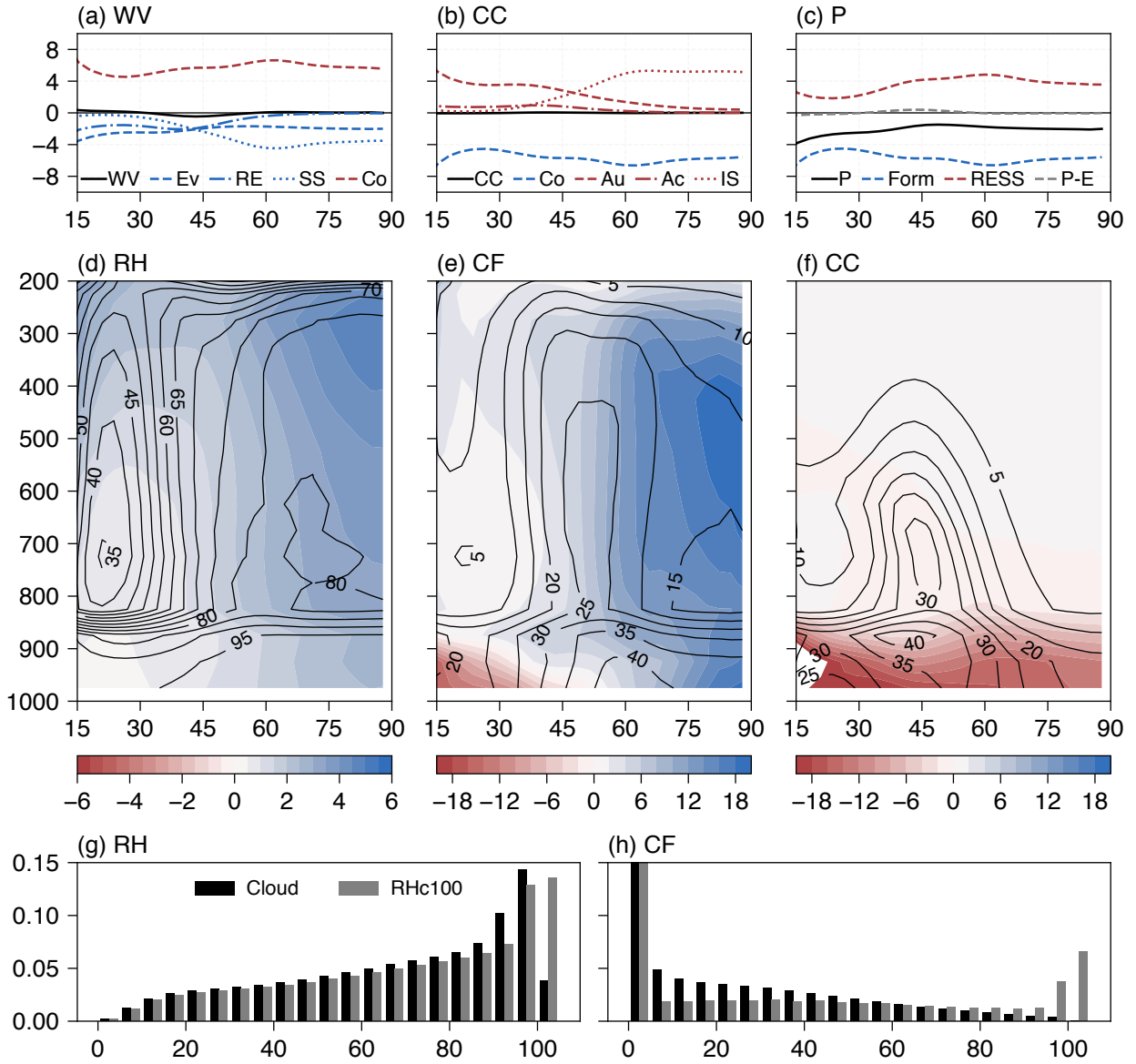
878 FIG. 2. Principal WV and CC sources and sinks for various model runs (see Table 1) represented as column-
 879 integrated average STET (15° - 90°) tendency values. For clarity, the smallest terms are conglomerated in an
 880 other (O) category. Processes shown are WV sources: surface evaporation (SE), rain evaporation (RE), and
 881 snow sublimation (SS); WV sink (CC source): LS condensation (Co); CC sinks: autoconversion (Au), accretion
 882 (Ac), and ice settling (IS). Base case saturation adjustment is labeled LS condensation. Tendency units (vertical
 883 axis) are $10^{-6} \text{ kg m}^{-2} \text{ s}^{-1}$. Percentages are given with respect to total source or sink category and may not add
 884 to 100% due to rounding.



885 FIG. 3. Diagram of the water cycle in the control cloud microphysics scheme (Cloud experiment). Water is
 886 cycled between four species (reservoirs): WV, CC, precipitation, and an assumed surface reservoir. The quantities
 887 shown are average STET (15° - 90°) tendency values with units of $10^{-6} \text{ kg m}^{-2} \text{ s}^{-1}$. Each reservoir shows either a
 888 balance (0.0) or an imbalance. Here, condensation comprises both LS condensation and deposition; evaporation
 889 comprises both LS evaporation and sublimation; formation includes autoconversion, accretion, ice settling, and
 890 melting of cloud ice to rain; and sedimentation represents formation processes minus RESS.



891 FIG. 4. Key variables in control runs: (a) RH difference (Cloud minus Base, %) as shading and Base RH
 892 as contours (5% spacing), (b) temperature (K) as shading and potential temperature as contours (5K spacing),
 893 (c) Cloud CF (%) as shading and Cloud RH as contours (5% spacing), (d) Cloud total CC ($10^{-6} \text{ kg kg}^{-1}$) as
 894 shading and liquid (solid) and ice (dashed) CC as contours ($5 \cdot 10^{-6} \text{ kg kg}^{-1}$ spacing). Variables have been zonally
 895 averaged, and the x- and y-axes are latitude and pressure (hPa), respectively.



896 FIG. 5. Key variable changes in RHc100 perturbation from Cloud control: absolute differences in zonally
 897 averaged (a) WV, (b) CC, and (c) precipitation (P) tendency terms (y-axis units of $10^{-6} \text{ kg m}^{-2} \text{ s}^{-1}$); absolute
 898 differences in (d) RH, (e) CF, and (f) CC as shading with Cloud values as contours (5%, 5%, and $5 \cdot 10^{-6} \text{ kg kg}^{-1}$
 899 spacing, respectively); comparison of normalized histograms of (g) RH and (h) CF in Cloud (black) and RHc100
 900 (grey) cases from daily data (x-axis units of %) between 15° and 90° and 850 and 250 hPa with the y-axis cut
 901 off at 0.15. For (a)-(c), WV, CC, and precipitation (P) tendency difference terms shown are as defined in Fig. 1,
 902 with units of $10^{-6} \text{ kg m}^{-2} \text{ s}^{-1}$ where a positive tendency difference denotes an increase in a WV/CC/P-increasing
 903 process or a decrease in a WV/CC/P-decreasing process. For (a)-(f) variables have been zonally averaged and
 904 the x-axis is latitude; for (d-f) the y-axis is pressure (hPa). For (g)-(h), histogram bins have widths of 5% and are
 905 all half-open except for the last bin: $[0, 5)$, $[5, 10)$, ..., $[100, 105]$.

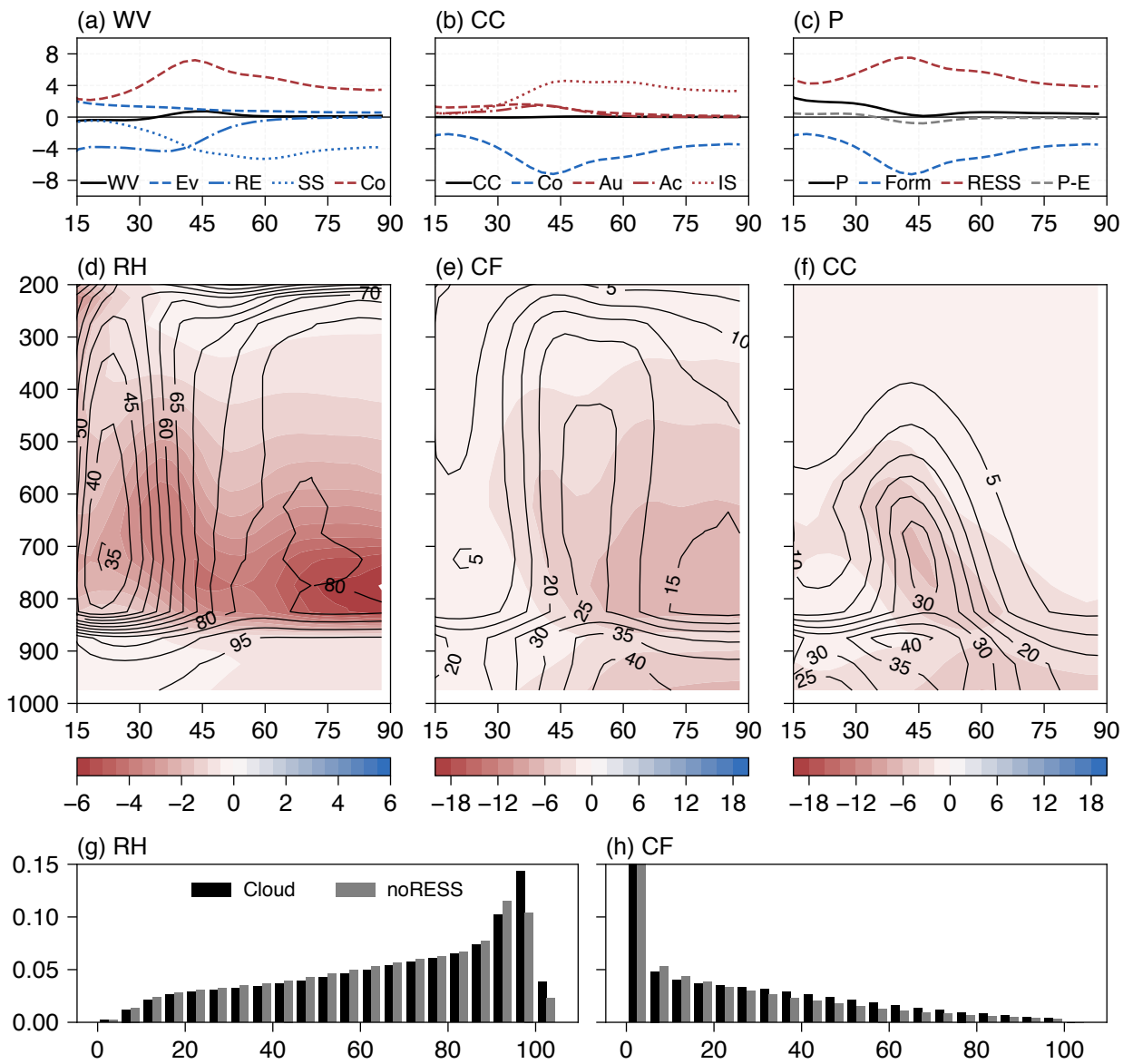
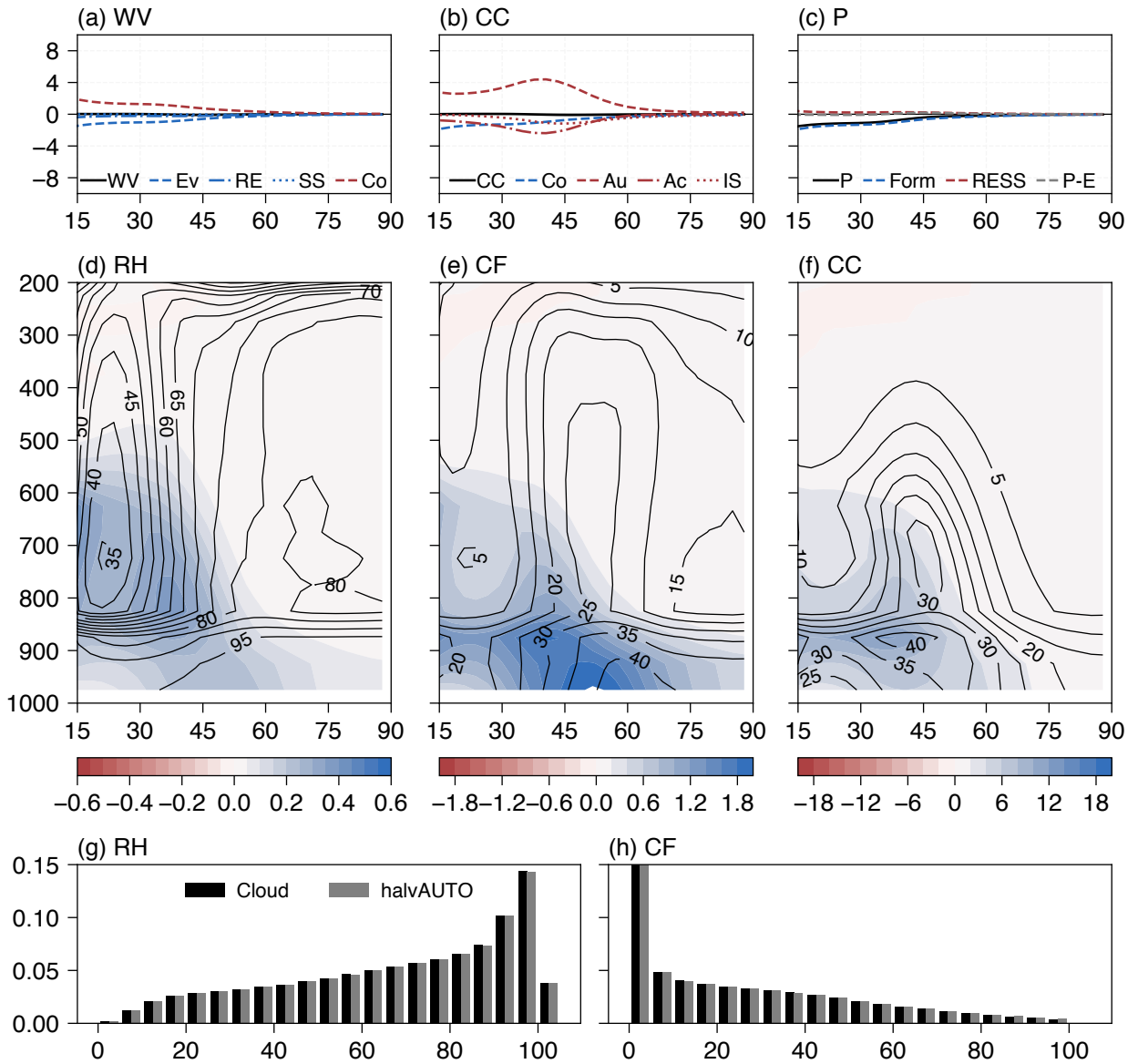
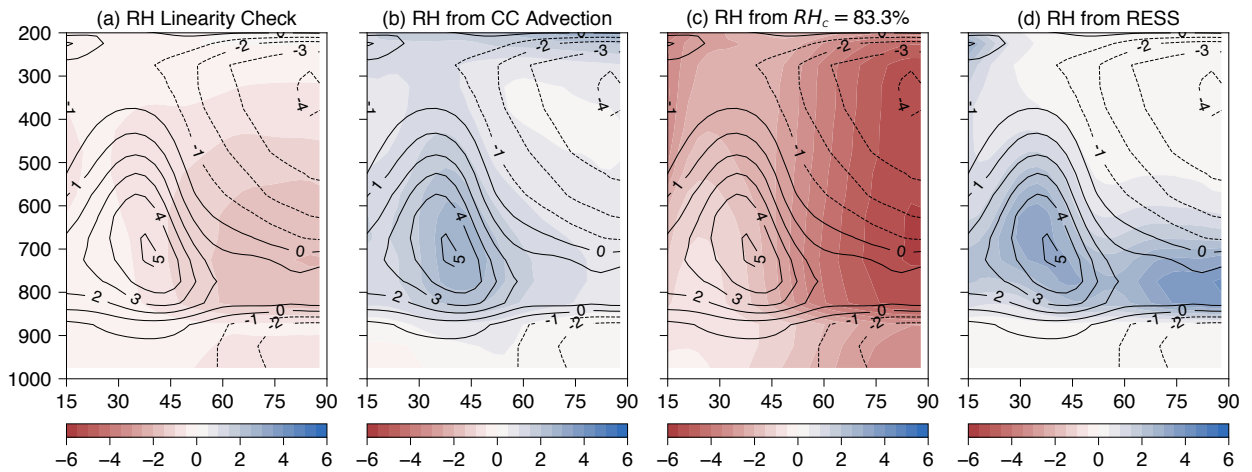


FIG. 6. As Fig. 5, but for noRESS perturbation.



906 FIG. 7. As Figs. 5 and 6, but for halvAUTO perturbation, except that the colorbar scale is reduced by a factor
 907 of 10 for (d) and (e).



908 FIG. 8. Comparison of absolute RH differences (%) between control cases and intermediate setups: (a) RHc100
 909 plus noRESS minus RHc100_noRESS minus Cloud [linearity check: should be 0 if $RH_c = 83.3\%$ and RESS
 910 effects sum linearly], (b) RHc100_noRESS minus Base [CC advection effect] as shading, (c) noRESS minus
 911 RHc100_noRESS [$RH_c = 83.3\%$ effect] as shading, (d) noRESS minus Base [RESS effect] as color shading.
 912 All contours are Cloud minus Base difference with a spacing of 1%.